

Quark Matter in a Strong Magnetic Background

Raoul Gatto and Marco Ruggieri

Abstract In this chapter, we discuss several aspects of the theory of strong interactions in presence of a strong magnetic background. In particular, we summarize our results on the effect of the magnetic background on chiral symmetry restoration and deconfinement at finite temperature. Moreover, we compute the magnetic susceptibility of the chiral condensate and the quark polarization at zero temperature. Our theoretical framework is given by chiral models: the Nambu-Jona-Lasinio (NJL), the Polyakov improved NJL (or PNJL) and the Quark-Meson (QM) models. We also compare our results with the ones obtained by other groups.

1 Introduction

Quantum Chromodynamics (QCD) is the gauge theory of strong interactions. The understanding of its vacuum, and how it is modified by a large temperature and/or a baryon density, is one of the most intriguing aspects of modern physics. However, it is very hard to get a full understanding of its properties, because its most important characteristics, namely chiral symmetry breaking and color confinement, have a non-perturbative origin, and the use of perturbative methods is useless. One of the best strategies to overcome this problem is offered by Lattice QCD simulations at zero chemical potential (see [1, 2, 3, 4] for several examples and see also references therein). At vanishing quark chemical potential, two crossovers take place in a broad range of temperatures; one for quark deconfinement, and another one for the (approximate) restoration of chiral symmetry.

Raoul Gatto

Departement de Physique Theorique, Universite de Geneve, CH-1211 Geneve 4, Switzerland. e-mail: raoul.gatto@unige.ch

Marco Ruggieri

Department of Astronomy and Physics, Catania University, Via S. Sofia 64, I-95125 Catania. e-mail: marco.ruggieri@lns.infn.it

An alternative approach to the physics of strong interactions, which is capable to capture some of the non-perturbative properties of the QCD vacuum, is the use of models. Among them, we will consider here the Nambu-Jona Lasinio (NJL) model [5], see Refs. [6] for reviews. In this gluon-less model, which was inspired by the microscopic theory of superconductivity, the QCD interactions are replaced by effective interactions, which are built in order to respect the global symmetries of QCD. Since gluons are absent in the NJL model, it is not a gauge theory. However, it shares the global symmetries of the QCD action; moreover, the parameters of the NJL model are fixed to reproduce some phenomenological quantity of the QCD vacuum. Therefore, it is the main characteristics of its phase diagram should represent, at least qualitatively, those of QCD.

The other side of the NJL model is that it lacks confinement. The latter, in the case of a pure gauge theory, can be described in terms of the center symmetry of the color gauge group and of the Polyakov loop [7], which is an order parameter for the center symmetry. Motivated by this property, the Polyakov extended Nambu-Jona Lasinio model (PNJL model) has been introduced [8, 9], in which the concept of statistical confinement replaces that of the true confinement of QCD, and an effective interaction among the chiral condensate and the Polyakov loop is achieved by a covariant coupling of quarks with a background temporal gluon field. In the literature there are several studies on the PNJL model, see Refs. [10, 11, 12, 13, 14, 15, 15, 17, 18, 19, 20, 21, 22, 23, 24, 25] and references therein.

In this Chapter, we make use of the PNJL model to study the interplay between chiral symmetry breaking and deconfinement in a *strong magnetic background*. Moreover, we compute several quantities which are relevant for the phenomenology of strong interactions physics in presence of a magnetic background. These topics are widely studied in the literature using many theoretical approaches. Lattice studies on the response to external magnetic (and chromo-magnetic) fields can be found in [26, 27, 28, 29, 30, 66, 67]. Previous studies of QCD in magnetic fields, and of QCD-like theories as well, can be found in Refs. [31, 33, 34, 35, 77]. Self-consistent model calculations of deconfinement pseudo-critical temperature in magnetic field have been performed [36, 73, 38].

An important motivation for these kind of studies is phenomenological. In fact, strong magnetic fields are produced in non-central heavy ion collisions [39, 40, 102]. For example, at the energy scale for RHIC it is found $eB_{max} \approx 5m_{\pi}^2$; for collisions at the LHC energy scale $eB_{max} \approx 15m_{\pi}^2$. In this case, it has been argued that the non-trivial topological structure of thermal QCD, namely the excitation of the strong sphalerons [103], locally changes the chirality of quarks; this is reflected to event-by-event charge separation, a phenomenon which is dubbed Chiral Magnetic Effect (CME) [39, 41, 42]. The possibility that the CME is observed in heavy ion collision experiments has motivated the study of strong interactions in presence of a chirality imbalance and a magnetic background, see [42, 104, 105, 106, 107, 108] and references therein. An experimental measurement of observables connected to charge separation has been reported by the ALICE collaboration in [109]. It is fair to say that realistic simulations of heavy ion collisions show that the magnetic fields have a

very short lifetime, and decay before the local equilibrium is reached in the fireball. Moreover, the magnetic field is highly inhomogeneous. Furthermore, electric fields are produced beside the magnetic fields. Therefore, in order to describe realistically hot matter produced in the collisions, one should take care of the aforementioned details. However, for simplicity we neglect them, and leave the (much harder) complete problem to future studies.

We mainly base the present Chapter on our previous works [60, 61, 95]. We firstly discuss chiral symmetry restoration in a strong magnetic background at finite temperature, using the PNJL model augmented with the eight-quark interaction [46, 47, 48, 49]. In this case we also compute the dressed Polyakov loop in a magnetic field. The scenario which turns out from our calculations is compatible with that of the magnetic catalysis, in which the magnetic field acts as a catalyzer for chiral symmetry breaking. Moreover, we discuss on the role of the entanglement NJL vertex on the separation between deconfinement and chiral symmetry restoration in the background field. Finally, we summarize our computation of the magnetic susceptibility of the chiral condensate and of quark polarization in a strong magnetic background at zero temperature. We base the latter analysis on the Quark-Meson (QM) model, which offers the simplest renormalizable extension of the NJL model. Throughout this Chapter we consider QCD in the vacuum, that is at zero baryon (as well as isospin) chemical potential. Computations at finite chemical potential are present in the literature, as we will mention in the main body of the Chapter.

2 The PNJL model with a magnetic background

In this Section, we mainly summarize the results obtained in [60, 61]. We consider quark matter modeled by the following Lagrangian density:

$$\begin{aligned} \mathcal{L} = & \bar{q} (i\gamma^\mu D_\mu - m_0) q + g_\sigma [(\bar{q}q)^2 + (\bar{q}i\gamma_5 \boldsymbol{\tau} q)^2] \\ & + g_8 [(\bar{q}q)^2 + (\bar{q}i\gamma_5 \boldsymbol{\tau} q)^2]^2, \end{aligned} \quad (1)$$

which corresponds to the NJL lagrangian with multi-quark interactions [46]. The covariant derivative embeds the quark coupling to the external magnetic field and to the background gluon field as well, as we will see explicitly below. In Eq. (1), q represents a quark field in the fundamental representation of color and flavor (indices are suppressed for notational simplicity); m_0 is the bare quark mass, which is fixed to reproduce the pion mass in the vacuum, $m_\pi = 139$ MeV. Our interaction in Eq. (1) consists of a four-quark term, whose coupling g_σ has inverse mass dimension of two, and an eight-quark term, whose coupling constant g_8 has inverse mass dimension of eight.

We are considering the effect of a strong magnetic background on chiral symmetry restoration as well as deconfinement at finite temperature. We assume the magnetic field to be along the positive z -axis; we chose to work in the Landau gauge, specified by the vector potential $\mathbf{A} = (0, Bx, 0)$.

To compute a temperature for the deconfinement crossover, we use the expectation value of the Polyakov loop, that we denote by L . In order to compute L we introduce a static, homogeneous and Euclidean background temporal gluon field, $A_0 = iA_4 = i\lambda_a A_4^a$, coupled minimally to the quarks via the QCD covariant derivative [9]. Then

$$L = \frac{1}{3} \text{Tr}_c \exp(i\beta \lambda_a A_4^a) , \quad (2)$$

where $\beta = 1/T$. In the Polyakov gauge, which is convenient for this study, $A_0 = i\lambda_3 \phi + i\lambda_8 \phi^8$; moreover, we work at zero quark chemical potential, therefore we can take $L = L^\dagger$ from the beginning, which implies $A_4^8 = 0$. This choice is also motivated by the study of [73], where it is shown that the paramagnetic contribution of the quarks to the thermodynamic potential induces the breaking of the Z_3 symmetry, favoring the configurations with a real-valued Polyakov loop.

Besides the Polyakov loop, it is interesting to compute the dressed Polyakov loop [43]. In order to define this quantity, we work in a finite Euclidean volume with temperature extension $\beta = 1/T$. We take *twisted* fermion boundary conditions along the compact temporal direction,

$$q(\mathbf{x}, \beta) = e^{-i\varphi} q(\mathbf{x}, 0) , \quad \varphi \in [0, 2\pi] , \quad (3)$$

while for spatial directions the usual periodic boundary condition is taken. The canonical antiperiodic boundary condition for the quantization of fermions at finite temperature, is obtained by taking $\varphi = \pi$ in the previous equation. The dual quark condensate, $\tilde{\Sigma}_n$, is defined as

$$\tilde{\Sigma}_n(m, V) = \int_0^{2\pi} \frac{d\varphi}{2\pi} \frac{e^{-i\varphi n}}{V} \langle \bar{q}q \rangle_G , \quad (4)$$

where n is an integer. The expectation value $\langle \cdot \rangle_G$ denotes the path integral over gauge field configurations. An important point is that in the computation of the expectation value, the twisted boundary conditions acts only on the fermion determinant; the gauge fields are taken to be quantized with the canonical periodic boundary condition.

Using a lattice regularization, it has been shown in [43] that Eq. (4) can be expanded in terms of loops which wind n times along the compact time direction. In particular, the case $n = 1$ is called the *dressed Polyakov loop*; it corresponds to a sum of loops winding just once along the time direction. These correspond to the thin Polyakov loop (the loop with shortest length) plus higher order loops, the order being proportional to the length of the loop. Each higher order loop is weighed by an inverse power of the quark mass. Because of the weight, in the infinite quark mass limit only the thin Polyakov loop survives; for this reason, the dressed Polyakov loop can be viewed as a mathematical dressing of the thin loop, by virtue of longer loops, the latter being more and more important as the quark mass tends to smaller values.

If we denote by z an element of the center of the color gauge group, then $\tilde{\Sigma}_n \rightarrow z^n \tilde{\Sigma}_n$. It then follows that, under the center of the symmetry group Z_3 , the

dressed Polyakov loop ($n = 1$) is an order parameter for the center symmetry, with the same transformation rule of the thin Polyakov loop. Since the center symmetry is spontaneously broken in the deconfinement phase and restored in the confinement phase [7] (in presence of dynamical quarks, it is only approximately restored), the dressed Polyakov loop can be regarded as an order parameter for the confinement-deconfinement transition as well.

2.1 The one-loop quark propagator

The evaluation of the bulk thermodynamic quantities requires we compute the quantum effective action of the model. This cannot be done exactly; hence we rely ourselves to the one-loop approximation for the partition function, which amounts to take the classical contribution plus the fermion determinant. At this level, the effect of the strong interactions is to modify the quark mass as follows:

$$M = m_0 - 2\sigma - 4\sigma^3 g_8 / g_\sigma^3, \quad (5)$$

where $\sigma = g_\sigma \langle \bar{q}q \rangle$. As a further simplification, we neglect condensation in the pseudoscalar channel. We notice that the quark mass depends only on the sum of the u and d chiral condensates; therefore the mean field quark mass does not depend on the flavor.

To write the one-loop quark propagator in the background of the magnetic field we make use of the Leung-Ritus-Wang method [55], which allows to expand the propagator on the complete and orthonormal set made of the eigenfunctions of a charged fermion in a homogeneous and static magnetic field. This is a well known procedure, discussed many times in the literature, see for example [56, 57, 59, 58]; therefore it is enough to quote the final result:

$$S_f(x, y) = \sum_{k=0}^{\infty} \int \frac{d p_0 d p_2 d p_3}{(2\pi)^4} E_P(x) \Lambda_k \frac{1}{P \cdot \gamma - M} \bar{E}_P(y), \quad (6)$$

where $E_P(x)$ corresponds to the eigenfunction of a charged fermion in magnetic field, and $\bar{E}_P(x) \equiv \gamma_0 (E_P(x))^\dagger \gamma_0$. In the above equation,

$$P = (p_0 + iA_4, 0, \mathcal{Q} \sqrt{2k|Q_f eB|}, p_z), \quad (7)$$

where $k = 0, 1, 2, \dots$ labels the k^{th} Landau level, and $\mathcal{Q} \equiv \text{sign}(Q_f)$, with Q_f denoting the charge of the flavor f ; Λ_k is a projector in Dirac space which keeps into account the degeneracy of the Landau levels; it is given by

$$\Lambda_k = \delta_{k0} [\mathcal{P}_+ \delta_{\mathcal{Q}, +1} + \mathcal{P}_- \delta_{\mathcal{Q}, -1}] + (1 - \delta_{k0}) I, \quad (8)$$

where \mathcal{P}_\pm are spin projectors and I is the identity matrix in Dirac spinor indices. The propagator in Eq. (6) has a non-trivial color structure, due to the coupling to the background gauge field, see Eq. (7).

It is useful to write down explicitly the expression of the chiral condensates for the flavor f with $f = u, d$. The chiral condensate is easily computed by taking minus the trace of the f -quark propagator. It is easy to show that the following equation holds:

$$\langle \bar{f}f \rangle = -N_c \frac{|Q_f eB|}{2\pi} \sum_{k=0}^{\infty} \beta_k \int \frac{dp_z}{2\pi} \frac{M_f}{\omega_f} \mathcal{C}(L, \bar{L}, T|p_z, k) . \quad (9)$$

Here,

$$\mathcal{C}(L, \bar{L}, T|p_z, k) = U_\Lambda - 2\mathcal{N}(L, \bar{L}, T|p_z, k) , \quad (10)$$

and \mathcal{N} denotes the statistically confining Fermi distribution function,

$$\mathcal{C}(L, \bar{L}, T|p_z, k) = \frac{1 + 2Le^{\beta\omega_f} + Le^{2\beta\omega_f}}{1 + 3Le^{\beta\omega_f} + 3Le^{2\beta\omega_f} + e^{3\beta\omega_f}} , \quad (11)$$

where

$$\omega_f^2 = p_z^2 + 2|Q_f eB|k + M^2 . \quad (12)$$

The first and the second addenda in the r.h.s. of Eq. (27) correspond to the vacuum and the thermal fluctuations contribution to the chiral condensate, respectively. The coefficient $\beta_k = 2 - \delta_{k0}$ keeps into account the degeneracy of the Landau levels. The vacuum contribution is ultraviolet divergent. In order to regularize it, we adopt a smooth regulator U_Λ , which is more suitable, from the numerical point of view, in our model calculation with respect to the hard-cutoff which is used in analogous calculations without magnetic field. We chose

$$U_\Lambda = \frac{\Lambda^{2N}}{\Lambda^{2N} + (p_z^2 + 2|Q_f eB|k)^N} . \quad (13)$$

2.2 The one-loop thermodynamic potential

The one-loop thermodynamic potential of quark matter in external fields has been discussed in [36, 38], in the case of canonical antiperiodic boundary conditions; following [21], it is easy to generalize it to the more general case of twisted boundary conditions:

$$\begin{aligned}
\Omega &= \mathcal{U}(L, \bar{L}, T) + \frac{\sigma^2}{g\sigma} + \frac{3\sigma^4 g_8}{g\sigma^4} - \sum_{f=u,d} \frac{|Q_f eB|}{2\pi} \sum_k \beta_k \int_{-\infty}^{+\infty} \frac{dp_z}{2\pi} g_\Lambda(p_z, k) \omega_k(p_z) \\
&- T \sum_{f=u,d} \frac{|Q_f eB|}{2\pi} \sum_k \beta_k \int_{-\infty}^{+\infty} \frac{dp_z}{2\pi} \log \left(1 + 3Le^{-\beta\mathcal{E}_-} + 3\bar{L}e^{-2\beta\mathcal{E}_-} + e^{-3\beta\mathcal{E}_-} \right) \\
&- T \sum_{f=u,d} \frac{|Q_f eB|}{2\pi} \sum_k \beta_k \int_{-\infty}^{+\infty} \frac{dp_z}{2\pi} \log \left(1 + 3\bar{L}e^{-\beta\mathcal{E}_+} + 3Le^{-2\beta\mathcal{E}_+} + e^{-3\beta\mathcal{E}_+} \right).
\end{aligned} \tag{14}$$

In the previous equation the arguments of the thermal exponentials are defined as

$$\mathcal{E}_\pm = \omega_f(p_z) \pm \frac{i(\varphi - \pi)}{\beta}, \tag{15}$$

with φ defined in Eq. (3).

The potential term $\mathcal{U}[L, \bar{L}, T]$ in Eq. (14) is built by hand in order to reproduce the pure gluonic lattice data [10]. Among several different potential choices [50] we adopt the following logarithmic form [9, 10],

$$\frac{\mathcal{U}[L, \bar{L}, T]}{T^4} = -\frac{a(T)}{2} \bar{L}L + b(T) \ln[1 - 6\bar{L}L + 4(\bar{L}^3 + L^3) - 3(\bar{L}L)^2], \tag{16}$$

with three model parameters (one of four is constrained by the Stefan-Boltzmann limit),

$$\begin{aligned}
a(T) &= a_0 + a_1 \left(\frac{T_0}{T} \right) + a_2 \left(\frac{T_0}{T} \right)^2, \\
b(T) &= b_3 \left(\frac{T_0}{T} \right)^3.
\end{aligned} \tag{17}$$

The standard choice of the parameters reads [10];

$$a_0 = 3.51, \quad a_1 = -2.47, \quad a_2 = 15.2, \quad b_3 = -1.75. \tag{18}$$

The parameter T_0 in Eq. (16) sets the deconfinement scale in the pure gauge theory, i.e. $T_c = 270$ MeV.

3 Numerical results

In this Section, we show our results. The main goal to achieve numerically is the solution of the gap equations,

$$\frac{\partial \Omega}{\partial \sigma} = 0, \quad \frac{\partial \Omega}{\partial L} = 0. \tag{19}$$

Table 1 Parameters of the model for the two choices of the UV-regulator.

	Λ (MeV)	m_0 (MeV)	g_σ (MeV) ⁻²	g_8 (MeV) ⁻⁸
$N = 5$	588.657	5.61	5×10^{-6}	6×10^{-22}

This is done by using a globally convergent algorithm with backtrack [51]. From the very definition of the dressed Polyakov loop, Eq. (4), the twisted boundary condition, Eq. (3), must be imposed only in D_φ . Therefore, we firstly compute the expectation value of the Polyakov loop and to the chiral condensate, taking $\varphi = \pi$. Then, in order to compute the dressed Polyakov loop, we compute the φ -dependent chiral condensate using the first of Eq. (19), keeping the expectation value of the Polyakov loop fixed at its value at $\varphi = \pi$ [21].

Following [60, 61] we report results obtained using the UV-regulator with $N = 5$. As expected, in the other cases no different qualitative results are found; the parameter set is specified in Table 1. In the case $N = 5$, they are obtained by the requirements that the vacuum pion mass is $m_\pi = 139$ MeV, the pion decay constant $f_\pi = 92.4$ MeV and the vacuum chiral condensate $\langle \bar{u}u \rangle \approx (-241 \text{ MeV})^3$. In this case, the chiral and deconfinement pseudo-critical temperatures at zero magnetic field are $T_0^X = T_0^P = 175$ MeV.

The main effect of the eight-quark interaction in Eq. (1) is to lower the pseudo-critical temperature of the crossovers. This has been already discussed several times in the literature [47, 46], in the context of both the NJL and the PNJL models. Therefore, it is not necessary to discuss it further here, while at the same time we prefer to stress the results that have not been discussed yet.

In order to identify the pseudo-critical temperatures, we have define the *effective susceptibilities* as

$$\chi_A = (m_\pi)^g \left| \frac{dA}{dT} \right|, \quad A = \sigma, P, \Sigma_1. \quad (20)$$

Strictly speaking, the quantities defined in the previous equation are not true susceptibilities. Nevertheless, they allow to represent faithfully the pseudo-critical region, that is, the range in temperature in which the various crossovers take place. Therefore, for our purposes it is enough to compute these quantities. In Equation (20), the appropriate power of m_π is introduced just for a matter of convenience, in order to have a dimensionless quantity; therefore, $g = 0$ if $A = \sigma, \Sigma_1$, and $g = 1$ if $A = P$.

3.1 Condensates and dressed Polyakov loop

From now on, we fix $N = 5$ unless specified. The results for this case are collected in the form of surface plots in Fig. 1. In more detail, in the figure we plot the chiral condensate $S \equiv (\sigma/2)^{1/3}$, the expectation value of the Polyakov loop, and the dressed Polyakov loop Σ_1 , as a function of temperature and magnetic field.

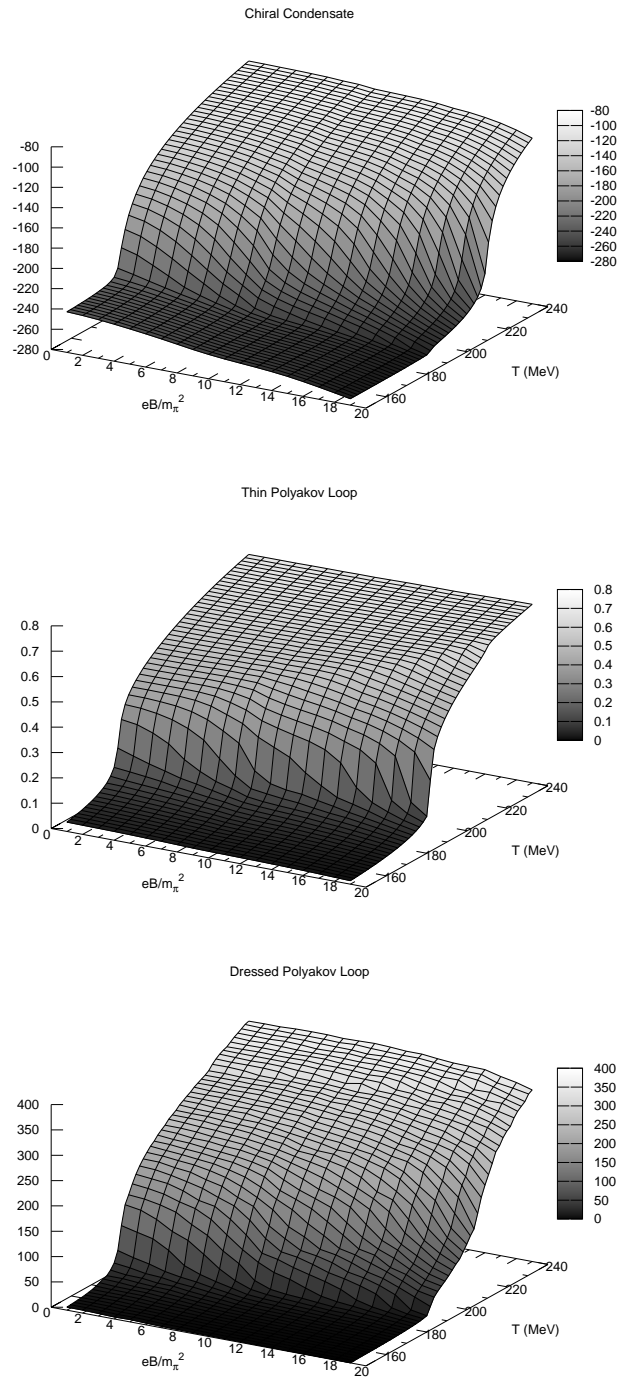


Fig. 1 Chiral condensate, Polyakov loop and dressed Polyakov loop as a function of temperature and magnetic field, for the case $N = 5$. From Ref. [61]. Copyright(2012) by the American Physical Society.

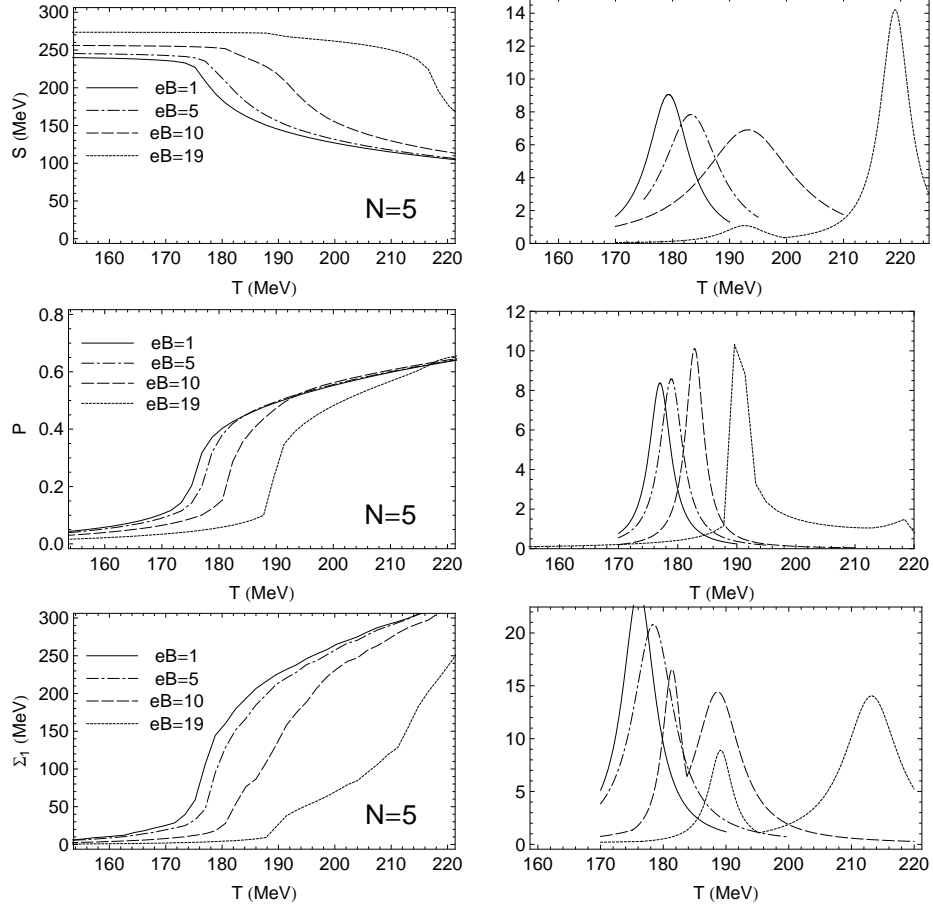


Fig. 2 *Left panel.* Chiral condensate S (upper panel), Polyakov loop (middle panel) and Σ_1 (lower panel) as a function of temperature, for several values of the applied magnetic field strength, measured in units of m_π^2 . *Right panel.* Effective susceptibilities, defined in Eq. (20), as a function of temperature, for several values of eB . Conventions for lines are the same as in the left panel. From Ref. [61]. Copyright(2012) by the American Physical Society.

We slice the surface plots in Fig. 1 at fixed value of the magnetic field strength, and show the results in Fig. 2, where we plot the chiral condensate (upper panel), the Polyakov loop (middle panel) and Σ_1 (lower panel) as a function of temperature, for several values of the applied magnetic field strength, measured in units of m_π^2 . In the right panel, we plot fits of the effective susceptibilities in the critical regions, as a function of temperature. The fits are obtained from the raw data, using Breit-Wigner-like fitting functions.

The qualitative behavior of the chiral condensate, and of the Polyakov loop as well, is similar to that found in a previous study within the PNJL model in the chiral

limit [36]. Quantitatively, the main difference with the case of the chiral limit, is that in the latter the chiral restoration at large temperature is a true second order phase transition (in other model calculations it has been reported that the phase transition might become of the first order at very large magnetic field strengths [35]). On the other hand, in the case under investigation, chiral symmetry is always broken explicitly because of the bare quark masses; as a consequence, the second order phase transition is replaced by a crossover.

Another aspect is that the Polyakov loop crossover temperature is less sensitive to the strength of the magnetic field than the same quantity computed for the chiral condensate. It is useful, for illustration purpose, to quantify the net shift of the pseudo-critical temperatures, for the largest value of magnetic field we have studied, $eB = 19m_\pi^2$. In this case, if we take $N = 5$, then the two crossovers occur simultaneously at $eB = 0$, at the temperature $T_0^\chi = T_0^P = 175$ MeV; for $eB = 19m_\pi^2$, we find $T_\chi = 219$ MeV and $T_P = 190$ MeV. Therefore, the chiral crossover is shifted approximately by 25.1%, to be compared with the more modest shift of the Polyakov loop crossover, which is $\approx 8.6\%$. This aspect will be discussed further in the next Section, in which we will comment on the possibility of entanglement between the NJL coupling at finite temperature and the Polyakov loop.

In the lower panels of Figures. 1 and 2, we plot the dressed Polyakov loop as a function of temperature, for several values of eB . We have normalized Σ_1 multiplying the one defined in [43] by the NJL coupling constant. For small values of eB/m_π^2 , the behavior of Σ_1 as temperature is increased, is qualitatively similar to that at $eB = 0$, which has been discussed within effective models in [21, 45]. In particular, the dressed Polyakov loop is very small for temperatures below the pseudo-critical temperature of the simultaneous crossover. Then, it experiences a crossover in correspondence of the simultaneous Polyakov loop and chiral condensate crossovers. It eventually saturates at very large temperature (for example, in [21] the saturation occurs at a temperature of the order of 0.4 GeV, in agreement with the results of [45]). However, we do not push up our numerical calculation to such high temperature, because we expect that the effective model in that case is well beyond its range of validity.

As we increase the value of eB , as noticed previously, we observe a tiny splitting of the chiral and the Polyakov loop crossovers. Correspondingly, the qualitative behavior of the dressed Polyakov loop changes dramatically: the range of temperature in which the Σ_1 crossover takes place is enlarged, if compared to the thin temperature interval in which the crossover takes place at the lowest value of eB (compare the solid and the dotted lines in Fig. 2, as well as the the lower panel of Fig. 1).

On passing, we discuss briefly the effective susceptibility, $d\Sigma_1/dT$, plotted in the lower right panel of Fig. 2, since its qualitative behavior is very interesting. We observe a double peak structure, which we interpret as the fact that the dressed Polyakov loop is capable to feel (and hence, describe) both the crossovers. If we were to interpret Σ_1 as the order parameter for deconfinement, and the temperature with the largest susceptibility as the crossover pseudo-critical temperature, then we obtain almost simultaneous crossover even for very large magnetic field.

3.2 Entanglement of NJL coupling and Polyakov loop

In [62] it has been shown that the NJL vertex can be deduced under some assumption from the QCD action; following this derivation a non-local structure of the interaction turns out. An analogous conclusion is achieved in [63]. More important for our study, the NJL vertex acquires a non-trivial dependence on the phase of the Polyakov loop. Therefore, in the model we consider here, it is important to keep into account this dependence. Here we follow the phenomenological ansatz introduced in [53], that is

$$G = g_\sigma [1 - \alpha_1 L \bar{L} - \alpha_2 (L^3 + \bar{L}^3)] , \quad (21)$$

and we take $L = \bar{L}$. Moreover, we mainly discuss here the case without 8-quark interaction. The model with coupling constant specified in Eq. (21) is named Entangled-Polyakov improved-NJL model (EPNJL in the following) [53], since the vertex describes an entanglement between Polyakov loop and the interaction responsible for chiral symmetry breaking.

The functional form in the above equation is constrained by C and extended Z_3 symmetry. We refer to [53] for a more detailed discussion. The numerical values of α_1 and α_2 have been fixed in [53] by a best fit of the available Lattice data at zero and imaginary chemical potential of Ref. [64], which have been confirmed recently in [65]. In particular, the fitted data are the critical temperature at zero chemical potential, and the dependence of the Roberge-Weiss endpoint on the bare quark mass.

The values $\alpha_1 = \alpha_2 \equiv \alpha = 0.2 \pm 0.05$ have been obtained in [53] using a hard cutoff regularization scheme. We will focus mainly on the case $\alpha = 0.2$ as in [53]. In [60] we have verified that in the regularization scheme with the smooth cutoff, the results are in quantitative agreement with those of [53]. There, a detailed discussion of the role of α can be found as well (we will skip this discussion in this Chapter).

We plot in Fig 3 the chiral condensates of u and d quarks as a function of temperature, at $eB = 15m_\pi^2$ and $eB = 30m_\pi^2$. In the lower panel of the figure, we plot the expectation value of the Polyakov loop as a function of temperature. The condensates are measured in units of their value at zero magnetic field and zero temperature, namely $\sigma_0 \equiv \langle \bar{u}u \rangle = \langle \bar{d}d \rangle = (-253 \text{ MeV})^3$. They are computed by a two-step procedure: firstly we find the values of σ and L that minimize the thermodynamic potential; then, we make use of Eq. (27) to compute the expectation values of $\bar{u}u$ and $\bar{d}d$ in magnetic field. If we measure the strength of the crossover by the value of the peak of $|d\sigma/dT|$, it is obvious from the Figure that the chiral crossover becomes stronger and stronger as the strength of the magnetic field is increased, in agreement with [26].

The results in Fig 3 show that, identifying the deconfinement crossover with the temperature T_L at which dL/dT is maximum, and the chiral crossover with the temperature T_χ at which $|d\sigma/dT|$ is maximum, the two temperatures are very close also in a strong magnetic field. From the model point of view, it is easy to understand why deconfinement and chiral symmetry restoration are entangled also in strong magnetic field. As a matter of fact, using the data shown in Fig 3, it is possible to

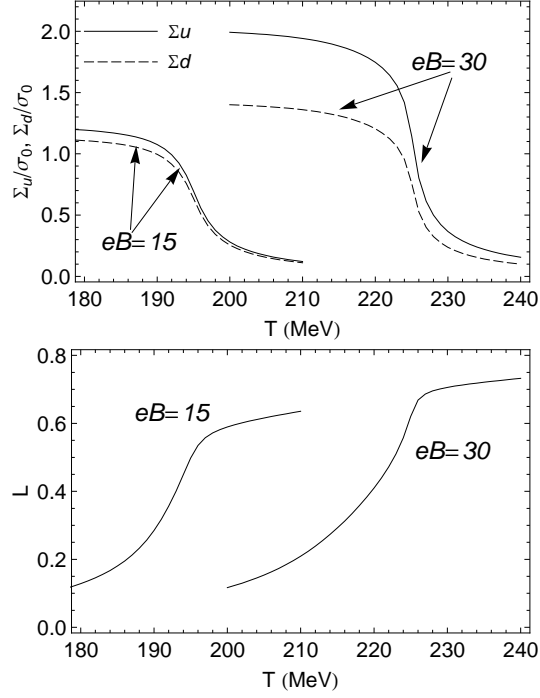


Fig. 3 *Upper panel:* Chiral condensates of u and d quarks as functions of temperatures in the pseudo-critical region, at $eB = 15m_\pi^2$ and $eB = 30m_\pi^2$. Condensates are measured in units of their value at zero magnetic field and zero temperature, namely $\sigma_0 = (-253 \text{ MeV})^3$. *Lower panel:* Polyakov loop expectation value as a function of temperature, at $eB = 15m_\pi^2$ and $eB = 30m_\pi^2$. Data correspond to $\alpha = 0.2$. From Ref. [61]. Copyright(2012) by American Physical Society.

compute the NJL coupling constant in the pseudo-critical region, which turns out to decrease of the 15% as a consequence of the deconfinement crossover. Therefore, the strength of the interaction responsible for the spontaneous chiral symmetry breaking is strongly affected by the deconfinement, with the obvious consequence that the numerical value of the chiral condensate drops down and the chiral crossover takes place. We have verified that the picture remains qualitatively and quantitatively unchanged if we perform a calculation at $eB = 30m_\pi^2$. In this case, we find $T_L = 224$ MeV and $T_\chi = 225$ MeV.

This result can be compared with the previous calculations [36], described also in the previous Section, in which the Polyakov loop dependence of the NJL coupling constant was not included. In [36] we worked in the chiral limit and we observed that the Polyakov loop crossover in the PNJL model is almost insensitive to the magnetic field; on the other hand, the chiral phase transition temperature was found to be very sensitive to the strength of the applied magnetic field, in agreement with the well known magnetic catalysis scenario [31]. This model prediction has been confirmed within the Polyakov extended quark-meson model in [73], when the contribution

from the vacuum fermion fluctuations to the energy density is kept into account ¹; we then obtained a similar result in [61], in which we turned from the chiral to the physical limit at which $m_\pi = 139$ MeV, and introduced the 8-quark term as well (PNJL₈ model, according to the nomenclature of [53]). The comparison with the results of the PNJL₈ model of [61] is interesting because the model considered there, was tuned in order to reproduce the Lattice data at zero and imaginary chemical potential [20], like the model we use in this study. Therefore, they share the property of describing the QCD thermodynamics at zero and imaginary chemical potential; it is therefore instructive to compare their predictions at finite eB .

For concreteness, in [61] we found $T_P = 185$ MeV and $T_\chi = 208$ MeV at $eB = 19m_\pi^2$, corresponding to a split of $\approx 12\%$. On the other hand, in the present calculation we measure a split of $\approx 1.5\%$ at the largest value of eB considered. Therefore, the results of the two models are in slight quantitative disagreement; this disagreement is then reflected in a slightly different phase diagram. We will draw the phase diagram of the two models in a next Section; however, since now it is easy to understand what the main difference consists in: the PNJL₈ model predicts some window in the $eB - T$ plane in which chiral symmetry is still broken by a chiral condensate, but deconfinement already took place. In the case of the EPNJL model, this window is shrunk to a very small one, because of the entanglement of the two crossovers at finite eB . On the other hand, it is worth to stress that the two models share an important qualitative feature: both chiral restoration and deconfinement temperatures are enhanced by a strong magnetic field; the latter conclusion is in qualitative agreement with the Lattice data of D’Elia *et al.* [26], but in disagreement with the more recent data of the Wuppertal-Budapest group [66, 67]. We will come back to a comparison with Lattice data, as well as with other computations, in the next Section.

4 Phase diagram in the $eB - T$ plane

In Fig. 4 we collect our data on the pseudo-critical temperatures for deconfinement and chiral symmetry restoration, in the form of a phase diagram in the $eB - T$ plane. In the upper panel we show the results obtained within the EPNJL model; in the lower panel, we plot the results of the PNJL₈ model, that are obtained using the fitting functions computed in [61]. In the figure, the magnetic field is measured in units of m_π^2 ; temperature is measured in units of the deconfinement pseudo-critical temperature at zero magnetic field, namely $T_{B=0} = 185.5$ MeV for the EPNJL model, and $T_{B=0} = 175$ MeV for the PNJL₈ model. For any value of eB , we identify the pseudo-critical temperature with the peak of the effective susceptibility.

¹ If the vacuum corrections are neglected, the deconfinement and chiral crossovers are found to be coincident even in very strong magnetic fields [73], but the critical temperature decreases as a function of eB ; this scenario is very interesting theoretically, but it seems excluded from the recent Lattice simulations [26].

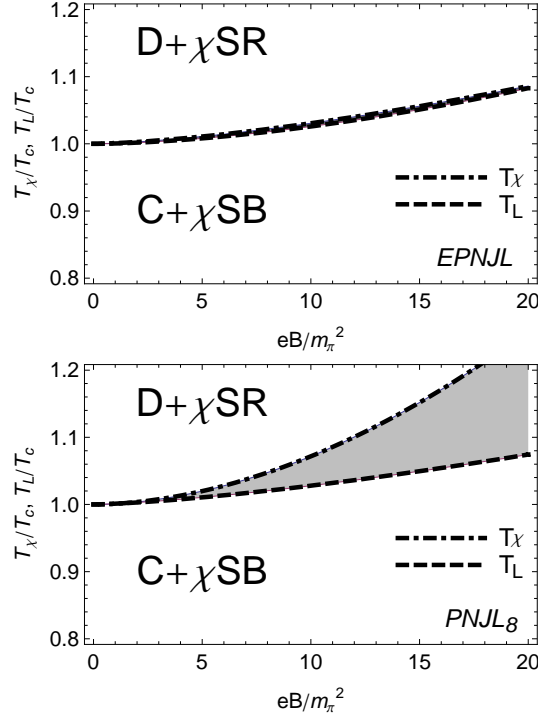


Fig. 4 *Upper panel:* Phase diagram in the $eB - T$ plane for the EPNJL model. Temperatures on the vertical axis are measured in units of the pseudo-critical temperature for deconfinement at $eB = 0$, namely $T_c = 185.5$ MeV. *Lower panel:* Phase diagram in the $eB - T$ plane for the PNJL₈ model. Temperatures on the vertical axis are measured in units of the pseudo-critical temperature for deconfinement at $eB = 0$, namely $T_c = 175$ MeV. In both the phase diagrams, T_χ, T_L correspond to the chiral and deconfinement pseudo-critical temperatures, respectively. The grey shaded region denotes the portion of phase diagram in which hot quark matter is deconfined and chiral symmetry is still broken spontaneously. From Ref. [61]. Copyright(2012) by American Physical Society.

It should be kept in mind, however, that the definition of a pseudo-critical temperature in this case is not unique, because of the crossover nature of the phenomena that we describe. Other satisfactory definitions include the temperature at which the order parameter reaches one half of its asymptotic value (which corresponds to the $T \rightarrow 0$ limit for the chiral condensate, and to the $T \rightarrow +\infty$ for the Polyakov loop), and the position of the peak in the true susceptibilities. The expectation is that the critical temperatures computed in these different ways differ from each other only of few percent. This can be confirmed concretely using the data in Fig. 3 at $eB = 30m_\pi^2$. Using the peak of the effective susceptibility we find $T_\chi = 225$ MeV and $T_L = 224$ MeV; on the other hand, using the half-value criterion, we find $T_\chi = 227$ MeV and $T_L = 222$ MeV, in very good agreement with the previous estimate. Therefore, the qualitative picture that we derive within our simple calculational scheme, namely

the entanglement of the two crossovers in a strong magnetic field, should not be affected by using different definitions of the critical temperatures.

Firstly we focus on the phase diagram of the EPNJL model. In the upper panel of Fig. 4, the dashed and dot-dashed lines correspond to the deconfinement and chiral symmetry restoration pseudo-critical temperatures, respectively. As a consequence of the entanglement, the two crossovers stay closed also in very strong magnetic field, as we have already discussed in the previous Section. The grey region in the Figure denotes a phase in which quark matter is (statistically) deconfined, but chiral symmetry is still broken. According to [68, 69], we can call this phase Constituent Quark Phase (CQP).

On the lower panel of Fig. 4 we have drawn the phase diagram for the PNJL₈ model based on Ref. [61] and discussed in the previous Section. The most astonishing feature of the phase diagram of the PNJL₈ model is the entity of the split among the deconfinement and the chiral restoration crossover. The difference with the result of the EPNJL model is that in the former, the entanglement with the Polyakov loop is neglected in the NJL coupling constant. As we have already mentioned in the previous Section, the maximum amount of split that we find within the EPNJL model, at the largest value of magnetic field considered here, is of the order of 2%; this number has to be compared with the split at $eB = 20m_\pi^2$ in the PNJL₈ model, namely $\approx 12\%$. The larger split causes a considerable portion of the phase diagram to be occupied by the CQP.

4.1 Comparison with other computations

In this Section we summarize the main results obtained in the literature, comparing them with the scenario depicted in our works. Before going ahead, it is useful to summarize the two main results obtained within our one-loop computations:

- The critical temperature for chiral symmetry restoration is *increased* by an external magnetic field;
- The split between deconfinement and chiral symmetry restoration temperatures in a strong magnetic background can *be reduced* if the entanglement vertex is considered.

The first conclusion is in agreement with most of the computations: calculations based on the quark-meson-model with and without quantum fluctuations [72, 71, 73, 75, 78], on chiral perturbation theory at finite temperature [70], on the PNJL model [36, 76], on the holographic correspondence [79, 80, 81, 77].

Besides models predictions, lattice computations of the critical temperatures in a magnetic background have been performed [26, 66, 67]. The computations of [26] have been performed with a pion mass of the order of 400 MeV, hence a little bit far from the physical limit. In this case, both the chiral symmetry restoration and the deconfinement temperatures are measured, and they are found to increase slightly with the magnetic field strength; moreover, the two transitions seem to be entangled

even at the largest value of the magnetic field considered in the study. On the other hand, in [66, 67] quark masses are chosen such that the lattice pion has its physical mass; in this case a non-trivial dependence of the critical temperature for chiral symmetry restoration on the magnetic field strength and the quark mass is found. In more detail, for the up and down quark condensates at the physical limit, the critical temperature decreases with the magnetic field strength. On the other hand, the critical temperature for the strange quark condensate is increased by the magnetic field, in agreement with the magnetic catalysis scenario. A measurement of the deconfinement temperature has not been performed. The results of [66, 67] are quite surprising since they reveal an unexpected role of the quark mass on the curvature of the critical line in the $eB - T$ plane.

Computations within the MIT bag model [74] do not have direct access to the chiral symmetry restoration, but to the deconfinement temperature. Within this model it is found that the critical temperature for deconfinement is a decreasing function of the external magnetic field strength. This conclusion is in agreement with a previous computation [35]. Furthermore, a decreasing temperature is found also within the quark-meson model if the fermion vacuum contribution is neglected [73]. If deconfinement and chiral symmetry restoration are entangled at finite magnetic field, then the MIT model based study would give some hint on the mechanism which makes the temperature for chiral symmetry restoration in a magnetic background lower than that at zero field. However, if this is the case, then the role of the quark mass on the dependence of the critical temperature on the magnetic field should be transparent. In our opinion, more study is needed to understand the puzzling behavior of T_c as a function of the magnetic field found on the Lattice: beside model computations, independent Lattice simulations should be performed, in order to confirm the results of [66, 67].

5 Polarization of the quark condensate

It has been realized that external fields can induce QCD condensates that are absent otherwise [82]. Here we focus on the magnetic moment, $\langle \bar{f} \Sigma^{\mu\nu} f \rangle$ where f denotes the fermion field of the flavor f -th, and $\Sigma^{\mu\nu} = -i(\gamma^\mu \gamma^\nu - \gamma^\nu \gamma^\mu)/2$. At small fields one can write, according to [82],

$$\langle \bar{f} \Sigma^{\mu\nu} f \rangle = \chi \langle \bar{f} f \rangle Q_f |eB|, \quad (22)$$

and χ is a constant independent of flavor, which is dubbed magnetic susceptibility of the quark condensate. In [82] it is proved that the role of the condensate (22) to QCD sum rules in external fields is significant, and it cannot be ignored. The quantity χ has been computed by means of special sum rules [82, 83, 84, 85, 86], OPE combined with Pion Dominance [87], holography [88, 89], instanton vacuum model [90], analytically from the zero mode of the Dirac operator in the background of a $SU(2)$ instanton [91], and on the Lattice in two color quenched simulations at

zero and finite temperature [92]. It has also been suggested that in the photoproduction of lepton pairs, the interference of the Drell-Yan amplitude with the amplitude of a process where the photon couples to quarks through its chiral-odd distribution amplitude, which is normalized to the magnetic susceptibility of the QCD vacuum, is possible [93]. This interference allows in principle to access the chiral odd transversity parton distribution in the proton. Therefore, this quantity is interesting both theoretically and phenomenologically. The several estimates, that we briefly review in Section III, lead to the numerical value of χ as follows:

$$\chi \langle \bar{f} f \rangle = 40 - 70 \text{ MeV} . \quad (23)$$

A second quantity, which embeds non-linear effects at large fields, is the polarization, μ_f , defined as

$$\mu_f = \left| \frac{\Sigma_f}{\langle \bar{f} f \rangle} \right| , \quad \Sigma_f = \langle \bar{f} \Sigma^{12} f \rangle , \quad (24)$$

which has been computed on the Lattice in [92] for a wide range of magnetic fields, in the framework of two-color QCD with quenched fermions. At small fields $\mu_f = |\chi Q_f e B|$ naturally; at large fields, non-linear effects dominate and an interesting saturation of μ_f to the asymptotic value $\mu_\infty = 1$ is measured. According to [92] the behavior of the polarization as a function of eB in the whole range examined, can be described by a simple inverse tangent function. Besides, magnetization of the QCD vacuum has been computed in the strong field limit in [94] using perturbative QCD, where it is found it grows as $B \log B$.

In [95] we compute the magnetic susceptibility of the quark condensate by means of the NJL and the QM models. This study is interesting because in the chiral models, it is possible to compute self-consistently the numerical values of the condensates as a function of eB , once the parameters are fixed to reproduce some characteristic of the QCD vacuum. We firstly perform a numerical study of the problem, which is then complemented by some analytic estimate of the same quantity within the renormalized QM model. Moreover, we compute the polarization of quarks at small as well as large fields, both numerically and analytically. In agreement with the Lattice results [92], we also measure a saturation of μ_f to one at large fields, in the case of the effective models. Our results push towards the interpretation of the saturation as a non-artifact of the Lattice. On the contrary, we can offer a simple physical understanding of this behavior, in terms of lowest Landau level dominance of the chiral condensate. As a matter of fact, using the simple equations of the models for the chiral condensate and for the magnetic moment, we can show that at large magnetic field μ_f has to saturate to one, because in this limit the higher Landau levels are expelled from the chiral condensate; as a consequence, the ratio of the two approaches one asymptotically.

We also obtain a saturation of the polarization within the renormalized QM model. There are some differences, however, in comparison with the results of the non-renormalized models. In the former case, the asymptotic value of μ_f is charge-dependent; moreover, the interpretation of the saturation as a lowest Landau level

(LLL) dominance is not straightforward, because the renormalized contribution of the higher Landau levels is important in the chiral condensate, even in the limit of very strong fields. It is possible that the results obtained within the renormalized model are a little bit far from true QCD. As a matter of fact, in the renormalized model we assume that the quark self-energy is independent on momentum; thus, when we take the limit of infinite quark momentum in the gap equation, and absorb the ultraviolet divergences by means of counterterms and renormalization conditions, we implicitly assume that that quark mass at large momenta is equal to its value at zero momentum. We know that this is not true, see for example [97, 96]: even in the renormalized theory, the quark self-energy naturally cuts off the large momenta, leading to LLL dominance in the traces of quark propagator which are relevant for our study. Nevertheless, it is worth to study this problem within the renormalized QM model in its simplest version, because it helps to understand the structure of this theory under the influence of a strong magnetic field.

In our calculations we neglect, for simplicity, the possible condensation of ρ -mesons at strong fields [98, 99]. Vector meson dominance [98] and the Sakai-Sugimoto model [100] suggest for the condensation a critical value of $eB_c \approx m_\rho^2 \approx 0.57 \text{ GeV}^2$, where m_ρ is the ρ -meson mass in the vacuum. Beside these, a NJL-based calculation within the lowest Landau level (LLL) approximation [99] predicts ρ -meson condensation at strong fields as well, even if in the latter case it is hard to estimate exactly eB_c , mainly because of the uncertainty of the parameters of the model. It would certainly be interesting to address this problem within our calculations, in which not only the LLL but also the higher Landau levels are considered, and in which the spontaneous breaking of chiral symmetry is kept into account self-consistently. However, this would complicate significantly the calculational setup. Therefore, for simplicity we leave this issue to a future project.

In [95] the computation of the polarization and of the magnetic susceptibility has been performed both within the NJL and the Quark-Meson (QM) models; the qualitative picture does not depend on the model considered. Moreover, within the QM model an analytical computation of the aforementioned quantities within the renormalized quantum effective potential is feasible (the NJL model, at least with a contact interaction as considered in [95], is not renormalizable). Therefore in this review chapter we limit ourselves to summarize the results obtained within the QM model, both numerical and analytical, deferring to the original reference for further details.

5.1 Non-renormalized Quark-Meson model results

In the QM model, a meson sector described by the linear sigma model lagrangian, is coupled to quarks via a Yukawa-type interaction. The model is renormalizable in $D = 3 + 1$ dimensions. However, since we adopt the point of view of it as an effective description of QCD, it is not necessary to use the renormalized version of the model itself. On the contrary, it is enough to fix an ultraviolet scale to cutoff the

divergent expectation values; the UV scale is then chosen phenomenologically, by requiring that the numerical value of the chiral condensate in the vacuum obtained within the model, is consistent with the results obtained from the sum rules [101]. This is a rough approximation of the QCD effective quark mass, which smoothly decays at large momenta [96, 97]. In Section IV we will use a renormalized version of the model, to derive semi-analytically some results in the two regimes of weak and strong fields.

The lagrangian density of the model is given by

$$\begin{aligned} \mathcal{L} = & \bar{q} [iD_\mu \gamma^\mu - g(\sigma + i\gamma_5 \boldsymbol{\tau} \cdot \boldsymbol{\pi})] q \\ & + \frac{1}{2} (\partial_\mu \sigma)^2 + \frac{1}{2} (\partial_\mu \boldsymbol{\pi})^2 - U(\sigma, \boldsymbol{\pi}) . \end{aligned} \quad (25)$$

In the above equation, q corresponds to a quark field in the fundamental representation of color group $SU(3)$ and flavor group $SU(2)$; the covariant derivative, $D_\mu = \partial_\mu - Q_f e A_\mu$, describes the coupling to the background magnetic field, where Q_f denotes the charge of the flavor f . Besides, σ , $\boldsymbol{\pi}$ correspond to the scalar singlet and the pseudo-scalar iso-triplet fields, respectively. The potential U describes tree-level interactions among the meson fields. In this article, we take its analytic form as

$$U(\sigma, \boldsymbol{\pi}) = \frac{\lambda}{4} (\sigma^2 + \boldsymbol{\pi}^2 - v^2)^2 - h\sigma , \quad (26)$$

where the first addendum is chiral invariant; the second one describes a soft explicit breaking of chiral symmetry, and it is thus responsible for the non-zero value of the pion mass. For $h = 0$, the interaction terms of the model are invariant under $SU(2)_V \otimes SU(2)_A \otimes U(1)_V$. This group is broken explicitly to $U(1)_V^3 \otimes U(1)_A^3 \otimes U(1)_V$ if the magnetic field is coupled to the quarks, because of the different electric charge of u and d quarks. Here, the superscript 3 in the V and A groups denotes the transformations generated by τ_3 , $\tau_3 \gamma_5$ respectively. Therefore, the chiral group in presence of a magnetic field is $U(1)_V^3 \otimes U(1)_A^3$. This group is then explicitly broken by the h -term to $U(1)_V^3$.

The formalism which is used to compute the magnetic susceptibility and the polarization of the quark condensate is similar to the one described in the previous Sections; therefore it is not necessary to give the details here. It is enough to write down the expressions for the chiral condensate at zero temperature,

$$\langle \bar{f} f \rangle = -N_c \frac{|Q_f e B|}{2\pi} \sum_{k=0}^{\infty} \beta_k \int \frac{dp_3}{2\pi} \frac{m_q}{\omega_k(p_3)} , \quad (27)$$

where the divergent integral on the r.h.s. of the above equation has to be understood regularized as in (13), and for the magnetic moment for the flavor f ,

$$\langle \bar{f} \Sigma^{\mu\nu} f \rangle = -\text{Tr}[\Sigma^{\mu\nu} S_f(x, x)] . \quad (28)$$

We take $\mathbf{B} = (0, 0, B)$; in this case, only $\Sigma^{12} \equiv \Sigma_f$ is non-vanishing. Using the properties of γ -matrices it is easy to show that only the Lowest Landau Level (LLL)

gives a non-vanishing contribution to the trace:

$$\Sigma_f = N_c \frac{Q_f |eB|}{2\pi} \int \frac{dp_3}{2\pi} \frac{m_q}{\omega_0(p_3)}, \quad (29)$$

where $\omega_0 = \omega_{k=0}$.

From Eq. (27) we notice that the prescription (13) is almost equivalent to the introduction of a running effective quark mass,

$$m_q = g\sigma\Theta(\Lambda^2 - p_3^2 - 2k|Q_f eB|), \quad (30)$$

that can be considered as a rough approximation to the effective running quark mass in QCD [97] which decays at large quark momenta, see also the discussion in [96]. Once the scale Λ is fixed, the Landau levels with $n \geq 1$ are removed from the chiral condensate if $eB \gg \Lambda^2$.

In the upper panel of Fig. 5, we plot the chiral condensates for u and d quarks, as a function of eB , for the QM model. The magnetic field splits the two quantities because of the different charge for the two quarks. The small oscillations, which are more evident for the case of the u -quark, are an artifact of the regularization scheme, and disappear if smoother regulators are used, see the discussion in [38]. In the regime of weak fields, our data are consistent with the scaling $\langle \bar{f}f \rangle \propto |eB|^2/M$ where M denotes some mass scale; in the strong field limit we find instead $\langle \bar{f}f \rangle \propto |eB|^{3/2}$. The behavior of the quark condensate as a function of magnetic field is in agreement with the magnetic catalysis scenario.

In the middle panel of Fig. 5 we plot our data for the expectation value of the magnetic moment. At weak fields, $\Sigma_f \propto |eB|$ as expected from Eq. (28). In the strong field limit, non-linearity arises because of the scaling of quark mass (or chiral condensate); we find $\Sigma_f \propto |eB|^{3/2}$ in this limit.

In the lower panel of Fig. 5 we plot our results for the polarization. Data are obtained by the previous ones, using the definition (24). At small fields, the polarization clearly grows linearly with the magnetic field. This is a natural consequence of the linear behavior of the magnetic moment as a function of eB for small fields, see Fig. 5. On the other hand, within the chiral models we measure a saturation of μ_f at large values of eB , to an asymptotic value $\mu_\infty = 1$. This conclusion remains unchanged if we consider the NJL model, and it is in agreement with the recent Lattice findings [92]. It should be noticed that, at least for the u -quark, saturation is achieved before the expected threshold for ρ -meson condensation [98, 99, 100]. Therefore, our expectation is that our result is stable also if vector meson condensation is considered.

The saturation to the asymptotic value $\mu_\infty = 1$ of polarization is naturally understood within the models we investigate, as a LLL dominance in the chiral condensate (i.e., full polarization). As a matter of fact, Σ_f and $\langle \bar{f}f \rangle$ turn out to be proportional in the strong field limit, since only the LLL gives a contribution to the latter, comparing Eq. (27) and (29) which imply

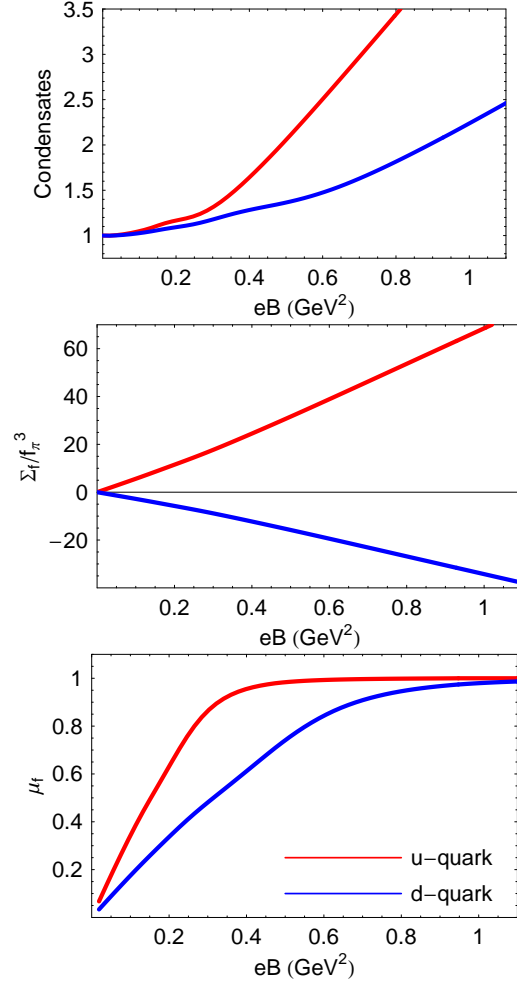


Fig. 5 *Upper panel.* Chiral condensates of u -quarks (red) and d -quarks (blue), in units of the same quantities at zero magnetic field, as a function of the magnetic field. *Middle panel.* Expectation value of the magnetic moment operator, in units of f_π^3 , as a function of eB . *Lower panel.* Polarization of u -quarks (red) and d -quarks (blue) as a function the magnetic field strength. From Ref. [95]. Copyright(2012) by American Physical Society.

$$\mu_f = 1 - \frac{\langle \bar{f}f \rangle_{\text{HLL}}}{\langle \bar{f}f \rangle}, \quad (31)$$

where $\langle \bar{f}f \rangle_{\text{HLL}}$ corresponds to the higher Landau levels contribution to the chiral condensate. In the strong field limit $\langle \bar{f}f \rangle_{\text{HLL}} \rightarrow 0$, see Eq. (27); hence, μ_f has to approach the asymptotic value $\mu_\infty = 1$. On the other hand, in the weak field limit $\langle \bar{f}f \rangle_{\text{HLL}} \rightarrow \langle \bar{f}f \rangle$ and the proportionality among Σ_f and $\langle \bar{f}f \rangle$ is lost.

At small fields $\mu_f = |\chi Q_f eB|$ from Eq. (22). Hence, we use the data on polarization at small fields, to obtain the numerical value of the magnetic susceptibility of the chiral condensate. Our results are as follows:

$$\chi \approx -4.3 \text{ GeV}^{-2}, \quad \text{NJL} \quad (32)$$

$$\chi \approx -5.25 \text{ GeV}^{-2}, \quad \text{QM} \quad (33)$$

respectively for the NJL model and the QM model. To obtain the numerical values above we have used data for eB up to $5m_\pi^2 \approx 0.1 \text{ GeV}^2$, which are then fit using a linear law. Using the numerical values of the chiral condensate in the two models, we obtain

$$\chi(\bar{f}f) \approx 69 \text{ MeV}, \quad \text{NJL} \quad (34)$$

$$\chi(\bar{f}f) \approx 65 \text{ MeV}, \quad \text{QM} \quad (35)$$

The numerical values of χ that we obtain within the effective models are in fair agreement with recent results, see Table I. In our model calculations, the role of the renormalization scale is played approximately by the ultraviolet cutoff, which is equal to 0.560 GeV in the QM model, and 0.627 GeV in the NJL model.

To facilitate the comparison with previous estimates, we review briefly the frameworks in which the results in Table I are obtained. In [87] the following result is found, within OPE combined with Pion Dominance (we follow when possible the notation used in [92]):

$$\chi^{PD} = -c_\chi \frac{N_c}{8\pi^2 F_\pi^2}, \quad \text{Pion Dominance} \quad (36)$$

with $F_\pi = \sqrt{2}f_\pi = 130.7 \text{ MeV}$ and $c_\chi = 2$; the estimate of [87] is done at a renormalization point $M = 0.5 \text{ GeV}$. It is remarkable that Eq. (36) has been reproduced recently within AdS/QCD approach in [89]. Probably, this is the result more comparable to our estimate, because the reference scales in [87] and in this article are very close. Within our model calculations we find $c_\chi^{NJL} = 1.93$ and $c_\chi^{QM} = 2.36$. Using the numerical value of F_π and c_χ we get $\chi^{PD} = -4.45 \text{ GeV}^{-2}$, which agrees within 3% with our NJL model result, and within 18% with our QM model result.

In [88] the authors find $c_\chi = 2.15$ within hard-wall holographic approach, at the scale $M \ll 1 \text{ GeV}$. The results of [88] are thus in very good parametric agreement with [87]; on the other hand, the numerical value of F_π in the holographic model is smaller than the one used in [87], pushing the holographic prediction for χ to slightly higher values than in [87]. However, the scale at which the result of [88] is valid should be much smaller than $M = 1 \text{ GeV}$, thus some quantitative disagreement with [87] is expected. As the authors have explained, it might be possible to tune the parameters of the holographic model, mainly the chiral condensate, to reproduce the correct value of F_π ; their numerical tests suggest that by changing the ratio $\langle \bar{f}f \rangle / m_\rho$ of a factor of 8, then the numerical value of c_χ is influenced only by a 5%.

Method	χ (GeV $^{-2}$)	Ren. Point (GeV)	Ref.
Sum rules	-8.6 ± 0.24	1	[82]
Sum rules	-5.7	0.5	[83]
Sum rules	-4.4 ± 0.4	1	[84]
Sum rules	-3.15 ± 0.3	1	[85]
Sum rules	-2.85 ± 0.5	1	[86]
OPE + Pion Dominance	$-N_c/(4\pi^2 F_\pi^2)$	0.5	[87]
Holography	$-1.075N_c/(4\pi^2 F_\pi^2)$	$\ll 1$	[88]
Holography	$-N_c/(4\pi^2 F_\pi^2)$	$\ll 1$	[89]
Instanton vacuum	-2.5 ± 0.15	1	[90]
Zero mode of Dirac Operator	-3.52	1	[91]
Lattice	-1.547(3)	2	[92]
NJL model	-4.3	0.63	This work
QM model	-5.25	0.56	This work

Table 2 Magnetic susceptibility of the quark condensate obtained within several theoretical approaches. In the table, $F_\pi = 130.7$ MeV. See the text for more details. Adapted from Ref. [95]. Copyright(2012) by American Physical Society.

It is therefore plausible that a best tuning makes the quantitative prediction of [88] much closer to the estimate of [87].

In [90] an estimate of χ within the instanton vacuum model has been performed beyond the chiral limit, both for light and for strange quarks (the result quoted in Table I corresponds to the light quarks; for the strange quark, $\chi_s/\chi_{u,d} \approx 0.15$ is found). Taking into account the numerical value of the chiral condensate in the instanton vacuum, the numerical estimate of [90] leads to $\chi = -2.5 \pm 0.15$ GeV $^{-2}$ at the scale $M = 1$ GeV. An analytic estimate within a similar framework has been obtained in [91], in which the zero-mode of the Dirac operator in the background of a $SU(2)$ instanton is used to compute the relevant expectation values. The result of [82] gives $\chi = -3.52$ GeV $^{-2}$ at $M \approx 1$ GeV.

In [92] the result $\chi = -1.547$ GeV $^{-2}$ is achieved within a two-color simulation with quenched fermions. It is interesting that in [92] the same quantity has been computed also at finite temperature in the confinement phase, at $T = 0.82T_c$, and the result seems to be independent on temperature. The reference scale of [92], determined by the inverse lattice spacing, is $M \approx 2$ GeV. Therefore the lattice results are not quantitatively comparable with our model calculation. However, they share an important feature with the results presented here, namely the saturation of the polarization at large values of the magnetic field. Finally, estimates of the magnetic susceptibility of the chiral condensate by means of several QCD sum rules exist [82, 83, 84, 85, 86]. The results are collected in Table I.

5.2 Results within the renormalized QM model

In this Section, we make semi-analytic estimates of the polarization and the magnetic susceptibility of the quark condensate, as well as for the chiral condensate in magnetic background, within the renormalized QM model. This is done with the scope to compare the predictions of the renormalized model with those of the effective models, in which an ultraviolet cutoff is introduced to mimic the QCD effective quark mass.

In the renormalized model, we allow the effective quark mass to be a constant in the whole range of momenta, which is different from what happens in QCD [97]. Thus, the higher Landau levels give a finite contribution to the vacuum chiral condensate even at very strong fields. This is easy to understand: the ultraviolet cutoff, Λ , in the renormalized model can be taken larger than any other mass scale, in particular $\Lambda \gg |eB|^{1/2}$; as a consequence, the condition $p_3^2 + 2n|eB| < \Lambda^2$ is satisfied taking into account many Landau levels even at very large eB . The contribution of the higher Landau levels, once renormalized, appears in the physical quantities to which we are interested here, in particular in the chiral condensate.

Since the computation is a little bit lengthy, it is useful to anticipate its several steps: firstly we perform regularization, and then renormalization, of the QEP at zero magnetic field (the corrections due to the magnetic field turn out to be free of ultraviolet divergences). Secondly, we solve analytically the gap equation for the σ condensate in the limit of weak fields, and semi-analytically in the opposite limit. The field-induced corrections to the QEP and to the solution of the gap equation are divergence-free in agreement with [32], and are therefore independent on the renormalization scheme adopted. Then, we compute the renormalized and self-consistent values of the chiral condensate and of the magnetic moment, as a function of eB , using the results for the gap equation. Within this theoretical framework, it is much more convenient to compute $\langle \bar{f}f \rangle$ and Σ_f by taking derivatives of the renormalized potential; in fact, the computation of the traces of the propagator in the renormalized model is much more involved if compared to the situation of the non-renormalized models, since in the former a non-perturbative (and non-trivial) renormalization procedure of composite local operators is required [?]. Finally, we estimate χ , as well as the behavior of the polarization as a function of eB .

5.2.1 Renormalization of the QEP

To begin with, we need to regularize the one-loop fermion contribution, namely

$$V_{1\text{-loop}}^{\text{fermion}} = -N_c \sum_f \frac{|Q_f eB|}{2\pi} \sum_{n=0}^{\infty} \beta_n \int_{-\infty}^{+\infty} \frac{dk}{2\pi} (k^2 + 2n|Q_f eB| + m_q^2)^{1/2}. \quad (37)$$

To this end, we define the function, $\mathcal{V}(s)$, of a complex variable, s , as

$$\mathcal{V}(s) = -N_c \sum_f \frac{|Q_f e B|}{2\pi} \sum_{n=0}^{\infty} \beta_n \int_{-\infty}^{+\infty} \frac{dk}{2\pi} (k^2 + 2n|Q_f e B| + m_q^2)^{\frac{1-s}{2}}. \quad (38)$$

The function $\mathcal{V}(s)$ can be analytically continued to $s = 0$. We define then $V_{1\text{-loop}}^{\text{fermion}} = \lim_{s \rightarrow 0^+} \mathcal{V}(s)$. After elementary integration over k , summation over n and taking the limit $s \rightarrow 0^+$, we obtain the result

$$\begin{aligned} V_{1\text{-loop}}^{\text{fermion}} &= N_c \sum_f \frac{(Q_f e B)^2}{4\pi^2} \left(\frac{2}{s} - \log(2|Q_f e B|) + a \right) B_2(q) \\ &\quad - N_c \sum_f \frac{(Q_f e B)^2}{2\pi^2} \zeta'(-1, q) \\ &\quad - N_c \sum_f \frac{|Q_f e B| m_q^2}{8\pi^2} \left(\frac{2}{s} - \log(m_q^2) + a \right), \end{aligned} \quad (39)$$

where we have subtracted terms which do not depend explicitly on the condensate. In the above equation, $\zeta(t, q)$ is the Hurwitz zeta function; for $\text{Re}(t) > 1$ and $\text{Re}(q) > 0$, it is defined by the series $\zeta(t, q) = \sum_{n=0}^{\infty} (n+q)^{-t}$; the series can be analytically continued to a meromorphic function defined in the complex plane $t \neq 1$. Moreover we have defined $q = (m_q^2 + 2|Q_f e B|)/2|Q_f e B|$; furthermore, $a = 1 - \gamma_E - \psi(-1/2)$, where γ_E is the Euler-Mascheroni number and ψ is the digamma function. The derivative $\zeta'(-1, q) = d\zeta(t, q)/dt$ is understood to be computed at $t = -1$.

The first two addenda in Eq. (39) arise from the higher Landau levels; on the other hand, the last addendum is the contribution of the LLL. The function B_2 is the second Bernoulli polynomial; using its explicit form, it is easy to show that the divergence in the LLL term in Eq. (39) is canceled by the analogous divergence in the first addendum of the same equation. It is interesting that the LLL contribution, which is in principle divergent, combines with a part of the contribution of the higher Landau levels, leading to a finite result. This can be interpreted as a renormalization of the LLL contribution. On the other hand, the remaining part arising from the higher Landau levels is still divergent; this divergence survives in the $\mathbf{B} \rightarrow 0$ limit, and is due to the usual divergence of the vacuum contribution. We then have

$$\begin{aligned} V_{1\text{-loop}}^{\text{fermion}} &= N_c \sum_f \frac{m_q^4}{16\pi^2} \left(\frac{2}{s} - \log(2|Q_f e B|) + a \right) \\ &\quad + N_c \sum_f \frac{|Q_f e B| m_q^2}{8\pi^2} \log \frac{m_q^2}{2|Q_f e B|} \\ &\quad - N_c \sum_f \frac{(Q_f e B)^2}{2\pi^2} \zeta'(-1, q). \end{aligned} \quad (40)$$

The renormalization procedure of the quantum effective potential is discussed in some detail in [95]. Here it is not necessary to discuss this procedure, and we just focus on the results.

5.2.2 Approximate solutions of the gap equation

Weak fields. In the weak field limit ($eB \ll m_q^2$) the correction due to the magnetic field to the quantum effective potential can be computed:

$$V_1 \approx -N_c \sum_f \frac{(Q_f eB)^2}{24\pi^2} \log \frac{m_q^2}{2|Q_f eB|} = -N_c \sum_f \frac{(Q_f eB)^2}{24\pi^2} \log \frac{m_q^2}{\mu^2}, \quad (41)$$

which is in agreement with the result of [32]. In the above equation we have followed the notation of [94] introducing an infrared scale μ , isolating and then subtracting the term which does not depend on the condensate. The scale μ is arbitrary, and we cannot determine it from first principles; on the other hand, it is irrelevant for the determination of the σ -condensate. We expect $\mu \approx f_\pi$ since this is the typical scale of chiral symmetry breaking in the model for the σ field.

In this limit, it is easy to obtain analytically the behavior of the constituent quark mass as a function of eB . As a matter of fact, we can expand the derivative of the QEP with respect to σ , around the solution at $B = 0$, writing $\langle \sigma \rangle = f_\pi + \delta\sigma$. Then, a straightforward evaluation leads to

$$m_q = g f_\pi \left(1 + \frac{5}{9} \frac{N_c}{12\pi^2 f_\pi^2 m_\sigma^2} (eB)^2 \right). \quad (42)$$

As anticipated, the scale μ is absent in the solution of the gap equation.

Strong fields. In the limit $eB \gg m_q^2$, we can find an asymptotic representation of V_1 by using the expansion $\zeta'(-1, q) = c_0 + c_1(q-1)$ valid for $q \approx 1$, with $c_0 = -0.17$ and $c_1 = -0.42$. Then we find

$$V_1 \approx -N_c \sum_f \frac{m_q^2}{8\pi^2} \left(\frac{m_q^2}{2} + |Q_f eB| \right) \log \frac{2|Q_f eB|}{m_q^2} - N_c \sum_f \frac{|Q_f eB| m_q^2}{2\pi^2} c_1, \quad (43)$$

where we have subtracted condensate-independent terms.

In the strong field limit it is not easy to find analytically an asymptotic representation for the sigma condensate as a function of eB ; therefore we solve the gap equation numerically, and then fit data with a convenient analytic form as follows:

$$m_q = b|eB|^{1/2} + \frac{c f_\pi^3}{|eB|}, \quad (44)$$

where $b = 0.32$ and $c = 32.78$. At large fields the quark mass grows as $|eB|^{1/2}$ as expected by dimensional analysis; this is a check of the equations that we use.

5.2.3 Evaluation of chiral condensate and magnetic moment

Chiral condensate. To compute the chiral condensate we follow a standard procedure: we introduce source term for $\bar{f}f$, namely a bare quark mass m_f , then take derivative of the effective potential with respect to m_f evaluated at $m_f = 0$. For the weak field case we obtain

$$\langle \bar{f}f \rangle = \langle \bar{f}f \rangle_0 - \frac{N_c}{12\pi^2} \frac{|Q_f eB|^2}{m_q}. \quad (45)$$

On the other hand, in the strong field limit we have

$$\langle \bar{f}f \rangle = -\frac{N_c m_q}{4\pi^2} (|Q_f eB| + m_q^2) \log \frac{2|Q_f eB|}{m_q^2}. \quad (46)$$

Using Equations (42) and (44), we show that the chiral condensate scales as $a + b(eB)^2$ for small fields, and as $|eB|^{3/2}$ for large fields.

Magnetic moment. Next we turn to the computation of the expectation value of the magnetic moment. The expression in terms of Landau levels is given by Eq. (29), which clearly shows that this quantity has a log-type divergence. In order to avoid a complicated renormalization procedure of a local composite operator, we notice that it is enough to take the minus derivative of V_1 with respect to \mathbf{B} to get magnetization, \mathcal{M} [94], then multiply by $2m/Q_f$ to get the magnetic moment. This procedure is very cheap, since the \mathbf{B} -dependent contributions to the effective potential are finite, and the resulting expectation value will turn out to be finite as well (that is, already renormalized).

In the case of weak fields, from Eq. (41) we find

$$\Sigma_f = N_c \frac{Q_f |eB| m_q}{6\pi^2} \log \frac{m_q^2}{\mu^2}. \quad (47)$$

On the other hand, in the strong field limit we get from Eq. (43)

$$\Sigma_f = N_c \frac{m_q^3}{4\pi^2} \log \frac{2|Q_f eB|}{m_q^2}. \quad (48)$$

The above result is in parametric agreement with the estimate of magnetization in [94]. In fact, $m_q^2 \approx |eB|$ in the strong field limit, which leads to a magnetization $\mathcal{M} \approx B \log B$.

Using the expansions for the sigma condensate at small and large values of the magnetic field strength, we argue that $\Sigma_f \approx |eB|$ in a weak field, and $\Sigma_f \approx |eB|^{3/2}$ in a strong field.

5.2.4 Computation of chiral magnetization and polarization

We can now estimate the magnetic susceptibility of the quark condensate and the polarization as a function of eB . For the former, we need to know the behavior of the magnetic moment for weak fields. From Eq. (47) and from the definition (22) we read

$$\chi\langle\bar{f}f\rangle = \frac{N_c m_q}{6\pi^2} \log \frac{m_q^2}{\mu^2} \equiv f(\mu). \quad (49)$$

The presence of the infrared scale μ makes the numerical estimate of χ uncertain; however, taking for it a value $\mu \approx f_\pi$, which is the typical scale of chiral symmetry breaking, we have $\chi\langle\bar{f}f\rangle \approx 44$ MeV, which is in agreement with the expected value, see Eq. (23).

Next we turn to the polarization. For weak fields we find trivially a linear dependence of μ_f on $|Q_f eB|$, with slope given by the absolute value of χ in Eq. (49). On the other hand, in the strong field limit we find, according to Eq. (48),

$$\mu_f \approx \frac{m_q^2}{m_q^2 + |Q_f eB|} \approx 1 - \frac{|Q_f|}{b + |Q_f|}, \quad (50)$$

where we have used Eq. (44). This result shows that the polarization saturates at large values of eB , but the asymptotic value depends on the flavor charge.

It is interesting to compare the result of the renormalized model with that of the effective models considered in the previous Section. In the former, the asymptotic value of μ_f is flavor-dependent; in the latter, $\mu_f \rightarrow 1$ independently on the value of the electric charge. Our interpretation of this difference is as follows: comparing Eq. (50) with the general model expectation, Eq. (31), we recognize in the factor $|Q_f|/(b + |Q_f|)$ the contribution of the higher Landau levels at zero temperature, which turns out to be finite and non-zero after the renormalization procedure. This contribution is then transmitted to the physical quantities that we have computed. The trace of the higher Landau levels is implicit in the solution of the gap equation in the strong field limit, namely the factor b in Eq. (44), and explicit in the additional $|Q_f|$ dependence in Eq. (50). A posteriori, this conclusion seems quite natural, because in the renormalization procedure we assume that the effective quark mass is independent of quark momentum, thus there is no cut of the large momenta in the gap equation (and in the equation for polarization as well). In the effective models considered in the first part of this article, on the other hand, the cutoff procedure is equivalent to have a momentum-dependent effective quark mass, $m_q = g\sigma\Theta(\Lambda^2 - p_3^2 - 2n|Q_f eB|)$, which naturally cuts off higher Landau levels when $eB \gg \Lambda^2$. At the end of the days, the expulsion of the higher Landau levels from the chiral condensate makes $\mu_f \rightarrow 1$ in the strong field limit. Our expectation is that if we allow the quark mass to run with momentum and decay rapidly at large momenta, mimicking the effective quark mass of QCD, higher Landau levels would be suppressed in the strong field limit, and the result (50) would tend to the result in Fig. 5.

6 Conclusions

In this Chapter we have summarized our results for the phase structure of quark matter in a strong magnetic background. Our theoretical investigative tools are chiral quark models improved with the Polyakov loop, which allow to study simultaneously chiral symmetry breaking and deconfinement.

The main motivation of this series of studies is of a phenomenological nature. In fact, it has been shown that huge magnetic fields are produced in non-central heavy ion collisions. These fields might trigger the P - and CP -odd process dubbed Chiral Magnetic Effect (CME). Therefore, in order to make quantitative estimates of the observables which are sensitive to the CME, it is extremely important to understand how hot quark matter behaves under the influence of a strong magnetic background. The other side of the coin is that simulations show these huge fields have a very short lifetime: therefore the present studies should take into account this time dependence. Moreover electric fields, which we have neglected so far, are also produced in the collisions. Finally, the electromagnetic fields considerably depend on space coordinates on the scale of the volume of the expanding fireball. This dependence has been ignored in our studies, since the magnetic background is taken to be homogeneous in space and constant in time.

Our results support the scenario of magnetic catalysis, which manifests itself in both an increase of the chiral condensate at zero temperature, and an increase of the critical temperature for chiral symmetry restoration. Moreover, depending on the interaction used, deconfinement may occur either together with chiral symmetry restoration, or anticipate it. The latter possibility, even if more fascinating than the former since it opens a window for the Constituent Quark Phase, seems to be excluded by lattice simulations.

Recent lattice simulations show that the critical temperature for chiral symmetry restoration, T_c , is strongly affected by the quark mass. In particular, for small quark masses (hence, for the u and d quarks) the critical temperature *decreases* with the magnetic field strength; on the other hand, T_c increases with the magnetic field strength for the s quark. As we have discussed in the main body of this Chapter, it seems that self-consistent computations within chiral quark models are not able to reproduce this feature, even when quantum fluctuations are taken into account. Thus, it remains an open problem to understand this unexpected behavior of T_c . Certainly independent simulations performed by other groups are necessary to confirm the present results.

We have also briefly summarized a computation of the magnetic susceptibility of the chiral condensate, χ , and of quark polarization, μ_f at zero temperature, based on the quark-meson model. The computed value of χ is in agreement with most of the previous estimates, and with experimental data. Moreover, this model gives a simple interpretation of the saturation of μ_f observed on the lattice: at very large magnetic field strength, the quarks occupy the lowest Landau level, expelling higher levels from the chiral condensate; hence, chiral condensate turns out to be proportional to the quark magnetic moment, making the ratio (that is, polarization) just a constant. In the case of the non-renormalized model, this constant turns out to be equal to one

and flavor independent; on the other hand, in the case of the renormalized model, the constant is flavor dependent. The latter result is easily understood: the renormalization procedure of the momentum independent interaction of the quark-meson model brings all the Landau levels into the renormalized chiral condensate. We expect that the replacement of the simple interaction discussed here with a non-local one, which should mimick the quark self-energy measured on the lattice, will make the expulsion of the higher Landau levels active also in the renormalized model, hence reproducing the results of the non-renormalized model.

Acknowledgements We are pleased to acknowledge the editors of this volume of *Lecture Notes in Physics* for their interest in our work and their kind invitation to contribute to the book. We also acknowledge K. Fukushima and M. Frasca for scientific collaborations which led to some of the results presented here.

References

1. P. de Forcrand and O. Philipsen, JHEP **0701**, 077 (2007) [arXiv:hep-lat/0607017]; JHEP **0811**, 012 (2008) [arXiv:0808.1096 [hep-lat]]; PoS **LATTICE2008**, 208 (2008) [arXiv:0811.3858 [hep-lat]].
2. Y. Aoki, Z. Fodor, S. D. Katz and K. K. Szabo, Phys. Lett. B **643**, 46 (2006) [arXiv:hep-lat/0609068]; Y. Aoki, S. Borsanyi, S. Durr, Z. Fodor, S. D. Katz, S. Krieg and K. K. Szabo, JHEP **0906**, 088 (2009) [arXiv:0903.4155 [hep-lat]].
3. A. Bazavov *et al.*, Phys. Rev. D **80**, 014504 (2009) [arXiv:0903.4379 [hep-lat]].
4. M. Cheng *et al.*, arXiv:0911.3450 [hep-lat].
5. Y. Nambu and G. Jona-Lasinio, Phys. Rev. **122**, 345 (1961); Y. Nambu and G. Jona-Lasinio, Phys. Rev. **124**, 246 (1961).
6. U. Vogl and W. Weise, Prog. Part. Nucl. Phys. **27**, 195 (1991); S. P. Klevansky, Rev. Mod. Phys. **64**, 649 (1992); T. Hatsuda and T. Kunihiro, Phys. Rept. **247**, 221 (1994); M. Buballa, Phys. Rept. **407**, 205 (2005).
7. A. M. Polyakov, Phys. Lett. B **72**, 477 (1978); L. Susskind, Phys. Rev. D **20**, 2610 (1979); B. Svetitsky and L. G. Yaffe, Nucl. Phys. B **210**, 423 (1982); B. Svetitsky, Phys. Rept. **132**, 1 (1986).
8. P. N. Meisinger and M. C. Ogilvie, Phys. Lett. B **379**, 163 (1996) [arXiv:hep-lat/9512011].
9. K. Fukushima, Phys. Lett. B **591**, 277 (2004) [arXiv:hep-ph/0310121].
10. C. Ratti, M. A. Thaler and W. Weise, Phys. Rev. D **73**, 014019 (2006).
11. S. Roessner, C. Ratti and W. Weise, Phys. Rev. D **75**, 034007 (2007).
12. E. Megias, E. Ruiz Arriola and L. L. Salcedo, Phys. Rev. D **74**, 114014 (2006); Eur. Phys. J. A **31**, 553 (2007) [arXiv:hep-ph/0610163];
13. C. Sasaki, B. Friman and K. Redlich, Phys. Rev. D **75**, 074013 (2007).
14. S. K. Ghosh, T. K. Mukherjee, M. G. Mustafa and R. Ray, Phys. Rev. D **77**, 094024 (2008).
15. K. Fukushima, Phys. Rev. D **77**, 114028 (2008) [Erratum-ibid. D **78**, 039902 (2008)]; M. Ciminale, R. Gatto, N. D. Ippolito, G. Nardulli and M. Ruggieri, Phys. Rev. D **77**, 054023 (2008); W. j. Fu, Z. Zhang and Y. x. Liu, Phys. Rev. D **77**, 014006 (2008); T. Hell, S. Rossner, M. Cristoforetti and W. Weise, Phys. Rev. D **81**, 074034 (2010).
16. L. McLerran and R. D. Pisarski, Nucl. Phys. A **796**, 83 (2007) [arXiv:0706.2191 [hep-ph]].
17. H. Abuki, R. Anglani, R. Gatto, G. Nardulli and M. Ruggieri, Phys. Rev. D **78**, 034034 (2008).
18. T. Kahara and K. Tuominen, arXiv:1006.3931 [hep-ph].
19. Y. Sakai, K. Kashiwa, H. Kouno and M. Yahiro, Phys. Rev. D **77**, 051901 (2008); Phys. Rev. D **78**, 036001 (2008).

20. Y. Sakai, K. Kashiwa, H. Kouno, M. Matsuzaki and M. Yahiro, arXiv:0902.0487 [hep-ph].
21. K. Kashiwa, H. Kouno and M. Yahiro, Phys. Rev. D **80**, 117901 (2009).
22. H. Abuki, M. Ciminale, R. Gatto, N. D. Ippolito, G. Nardulli and M. Ruggieri, Phys. Rev. D **78**, 014002 (2008); H. Abuki, M. Ciminale, R. Gatto and M. Ruggieri, Phys. Rev. D **79**, 034021 (2009) [arXiv:0811.1512 [hep-ph]].
23. T. Sasaki, Y. Sakai, H. Kouno and M. Yahiro, arXiv:1005.0910 [hep-ph].
24. T. Hell, S. Roessner, M. Cristoforetti and W. Weise, Phys. Rev. D **79**, 014022 (2009).
25. K. Kashiwa, H. Kouno, M. Matsuzaki and M. Yahiro, Phys. Lett. B **662**, 26 (2008) [arXiv:0710.2180 [hep-ph]].
26. M. D'Elia, S. Mukherjee and F. Sanfilippo, arXiv:1005.5365 [hep-lat].
27. P. V. Buividovich, M. N. Chernodub, E. V. Luschevskaya and M. I. Polikarpov, Phys. Rev. D **81**, 036007 (2010) [arXiv:0909.2350 [hep-ph]].
28. P. V. Buividovich, M. N. Chernodub, E. V. Luschevskaya and M. I. Polikarpov, Phys. Lett. B **682**, 484 (2010) [arXiv:0812.1740 [hep-lat]].
29. P. Cea and L. Cosmai, JHEP **0302**, 031 (2003) [arXiv:hep-lat/0204023]; P. Cea and L. Cosmai, JHEP **0508**, 079 (2005) [arXiv:hep-lat/0505007].
30. P. Cea, L. Cosmai and M. D'Elia, JHEP **0712**, 097 (2007) [arXiv:0707.1149 [hep-lat]].
31. S. P. Klevansky and R. H. Lemmer, Phys. Rev. D **39**, 3478 (1989); I. A. Shushpanov and A. V. Smilga, Phys. Lett. B **402**, 351 (1997) [arXiv:hep-ph/9703201]; D. N. Kabat, K. M. Lee and E. J. Weinberg, Phys. Rev. D **66**, 014004 (2002) [arXiv:hep-ph/0204120]; T. Inagaki, D. Kimura and T. Murata, Prog. Theor. Phys. **111**, 371 (2004) [arXiv:hep-ph/0312005]; T. D. Cohen, D. A. McGady and E. S. Werbos, Phys. Rev. C **76**, 055201 (2007) [arXiv:0706.3208 [hep-ph]]; K. Fukushima and H. J. Warringa, Phys. Rev. Lett. **100**, 032007 (2008) [arXiv:0707.3785 [hep-ph]]; J. L. Noronha and I. A. Shovkovy, Phys. Rev. D **76**, 105030 (2007) [arXiv:0708.0307 [hep-ph]].
32. H. Suganuma and T. Tatsumi, Annals Phys. **208**, 470 (1991).
33. V. P. Gusynin, V. A. Miransky and I. A. Shovkovy, Nucl. Phys. B **462**, 249 (1996) [arXiv:hep-ph/9509320]; Nucl. Phys. B **563**, 361 (1999) [arXiv:hep-ph/9908320]; G. W. Semenoff, I. A. Shovkovy and L. C. R. Wijewardhana, Phys. Rev. D **60**, 105024 (1999) [arXiv:hep-th/9905116]; V. A. Miransky and I. A. Shovkovy, Phys. Rev. D **66**, 045006 (2002) [arXiv:hep-ph/0205348].
34. K. G. Klimenko, Theor. Math. Phys. **89**, 1161 (1992) [Teor. Mat. Fiz. **89**, 211 (1991)]; K. G. Klimenko, Z. Phys. C **54**, 323 (1992); K. G. Klimenko, Theor. Math. Phys. **90**, 1 (1992) [Teor. Mat. Fiz. **90**, 3 (1992)].
35. N. O. Agasian and S. M. Fedorov, Phys. Lett. B **663**, 445 (2008) [arXiv:0803.3156 [hep-ph]]; E. S. Fraga and A. J. Mizher, Phys. Rev. D **78**, 025016 (2008) [arXiv:0804.1452 [hep-ph]].
36. K. Fukushima, M. Ruggieri and R. Gatto, arXiv:1003.0047 [hep-ph].
37. A. J. Mizher, M. N. Chernodub and E. S. Fraga, arXiv:1004.2712 [hep-ph].
38. L. Campanelli and M. Ruggieri, Phys. Rev. D **80**, 034014 (2009) [arXiv:0905.0853 [hep-ph]].
39. D. E. Kharzeev, L. D. McLerran and H. J. Warringa, Nucl. Phys. A **803**, 227 (2008) [arXiv:0711.0950 [hep-ph]].
40. V. Skokov, A. Y. Illarionov and V. Toneev, Int. J. Mod. Phys. A **24**, 5925 (2009) [arXiv:0907.1396 [nucl-th]].
41. P. V. Buividovich, M. N. Chernodub, E. V. Luschevskaya and M. I. Polikarpov, Phys. Rev. D **80**, 054503 (2009) [arXiv:0907.0494 [hep-lat]]; M. Abramczyk, T. Blum, G. Petropoulos and R. Zhou, arXiv:0911.1348 [hep-lat].
42. K. Fukushima, D. E. Kharzeev and H. J. Warringa, Phys. Rev. D **78**, 074033 (2008) [arXiv:0808.3382 [hep-ph]].
43. E. Bilgici, F. Bruckmann, C. Gattringer and C. Hagen, Phys. Rev. D **77**, 094007 (2008) [arXiv:0801.4051 [hep-lat]].
44. C. S. Fischer, Phys. Rev. Lett. **103**, 052003 (2009) [arXiv:0904.2700 [hep-ph]]; C. S. Fischer and J. A. Mueller, Phys. Rev. D **80**, 074029 (2009) [arXiv:0908.0007 [hep-ph]]; C. S. Fischer, A. Maas and J. A. Mueller, arXiv:1003.1960 [hep-ph].
45. T. K. Mukherjee, H. Chen and M. Huang, arXiv:1005.2482 [hep-ph].

46. A. A. Osipov, B. Hiller, J. Moreira, A. H. Blin and J. da Providencia, Phys. Lett. B **646**, 91 (2007) [arXiv:hep-ph/0612082].
47. K. Kashiwa, H. Kouno, T. Sakaguchi, M. Matsuzaki and M. Yahiro, Phys. Lett. B **647**, 446 (2007) [arXiv:nucl-th/0608078].
48. A. A. Osipov, B. Hiller and J. da Providencia, Phys. Lett. B **634**, 48 (2006) [arXiv:hep-ph/0508058].
49. A. A. Osipov, B. Hiller, A. H. Blin and J. da Providencia, Phys. Lett. B **650**, 262 (2007) [arXiv:hep-ph/0701090].
50. B. J. Schaefer, M. Wagner and J. Wambach, Phys. Rev. D **81**, 074013 (2010) [arXiv:0910.5628 [hep-ph]].
51. W. Press, S. A. Teukolsky, W. T. Vetterling and B. P. Flannery, *Numerical Recipes: The Art of Scientific Computing, Third Edition*, Cambridge University Press (2007).
52. V. Skokov, B. Friman, E. Nakano, K. Redlich and B. J. Schaefer, arXiv:1005.3166 [hep-ph].
53. Y. Sakai, T. Sasaki, H. Kouno and M. Yahiro, arXiv:1006.3648 [hep-ph].
54. M. Cristoforetti, T. Hell, B. Klein and W. Weise, arXiv:1002.2336 [hep-ph].
55. V. I. Ritus, Annals Phys. **69**, 555 (1972); C. N. Leung and S. Y. Wang, Nucl. Phys. B **747**, 266 (2006).
56. E. Elizalde, E. J. Ferrer and V. de la Incera, Annals Phys. **295**, 33 (2002); E. Elizalde, E. J. Ferrer and V. de la Incera, Phys. Rev. D **70**, 043012 (2004).
57. E. J. Ferrer, V. de la Incera and C. Manuel, Phys. Rev. Lett. **95**, 152002 (2005); E. J. Ferrer, V. de la Incera and C. Manuel, Nucl. Phys. B **747**, 88 (2006).
58. K. Fukushima and H. J. Warringa, Phys. Rev. Lett. **100**, 032007 (2008); J. L. Noronha and I. A. Shovkovy, Phys. Rev. D **76**, 105030 (2007).
59. K. Fukushima, D. E. Kharzeev and H. J. Warringa, Nucl. Phys. A **836**, 311 (2010).
60. R. Gatto and M. Ruggieri, Phys. Rev. D **83**, 034016 (2011).
61. R. Gatto and M. Ruggieri, Phys. Rev. D **82**, 054027 (2010).
62. K. I. Kondo, Phys. Rev. D **82**, 065024 (2010).
63. M. Frasca, arXiv:0803.0319 [hep-th]; arXiv:1002.4600 [hep-ph]; Phys. Rev. C **84**, 055208 (2011).
64. M. D'Elia and F. Sanfilippo, Phys. Rev. D **80**, 111501 (2009).
65. C. Bonati, G. Cossu, M. D'Elia and F. Sanfilippo, arXiv:1011.4515 [hep-lat].
66. G. S. Bali, F. Bruckmann, G. Endrodi, Z. Fodor, S. D. Katz and A. Schafer, arXiv:1206.4205 [hep-lat].
67. G. S. Bali, F. Bruckmann, G. Endrodi, Z. Fodor, S. D. Katz, S. Krieg, A. Schafer and K. K. Szabo, JHEP **1202**, 044 (2012).
68. J. Cleymans, K. Redlich, H. Satz and E. Suhonen, Z. Phys. C **33**, 151 (1986).
69. H. Kouno and F. Takagi, Z. Phys. C **42**, 209 (1989).
70. J. O. Andersen, arXiv:1205.6978 [hep-ph].
71. J. O. Andersen and R. Khan, Phys. Rev. D **85**, 065026 (2012).
72. J. O. Andersen and A. Tranberg, arXiv:1204.3360 [hep-ph].
73. A. J. Mizher, M. N. Chernodub and E. S. Fraga, Phys. Rev. D **82**, 105016 (2010).
74. E. S. Fraga and L. F. Palhares, arXiv:1201.5881 [hep-ph].
75. V. Skokov, Phys. Rev. D **85**, 034026 (2012).
76. K. Kashiwa, Phys. Rev. D **83**, 117901 (2011).
77. F. Preis, A. Rebhan and A. Schmitt, JHEP **1103**, 033 (2011).
78. K. Fukushima and J. M. Pawłowski, arXiv:1203.4330 [hep-ph].
79. O. Bergman, G. Lifschytz and M. Lippert, JHEP **0805**, 007 (2008).
80. C. V. Johnson and A. Kundu, JHEP **0812**, 053 (2008).
81. A. V. Zayakin, JHEP **0807**, 116 (2008).
82. B. L. Ioffe and A. V. Smilga, Nucl. Phys. B **232**, 109 (1984).
83. V. M. Belyaev and Y. I. Kogan, Yad. Fiz. **40**, 1035 (1984).
84. I. I. Balitsky, A. V. Kolesnichenko and A. V. Yung, Sov. J. Nucl. Phys. **41**, 178 (1985) [Yad. Fiz. **41**, 282 (1985)].
85. P. Ball, V. M. Braun and N. Kivel, Nucl. Phys. B **649**, 263 (2003).
86. J. Rohrwild, JHEP **0709**, 073 (2007).

87. A. Vainshtein, Phys. Lett. B **569**, 187 (2003).
88. A. Gorsky and A. Krikun, Phys. Rev. D **79**, 086015 (2009).
89. D. T. Son and N. Yamamoto, arXiv:1010.0718 [hep-ph].
90. H. C. Kim, M. Musakhanov and M. Siddikov, Phys. Lett. B **608**, 95 (2005)
91. B. L. Ioffe, Phys. Lett. B **678**, 512 (2009).
92. P. V. Buividovich, M. N. Chernodub, E. V. Luschevskaya and M. I. Polikarpov, Nucl. Phys. B **826**, 313 (2010).
93. B. Pire and L. Szymanowski, Phys. Rev. Lett. **103**, 072002 (2009).
94. T. D. Cohen and E. S. Werbos, Phys. Rev. C **80**, 015203 (2009).
95. M. Frasca and M. Ruggieri, Phys. Rev. D **83**, 094024 (2011).
96. K. Langfeld, C. Kettner and H. Reinhardt, Nucl. Phys. A **608**, 331 (1996).
97. H. D. Politzer, Nucl. Phys. B **117**, 397 (1976); Phys. Lett. B **116**, 171 (1982).
98. M. N. Chernodub, Phys. Rev. D **82**, 085011 (2010).
99. M. N. Chernodub, arXiv:1101.0117 [hep-ph].
100. N. Callebaut, D. Dudal and H. Verschelde, arXiv:1102.3103 [hep-ph].
101. H. G. Dosch and S. Narison, Phys. Lett. B **417**, 173 (1998); S. Narison, Phys. Rev. D **74**, 034013 (2006).
102. V. Voronyuk, V. D. Toneev, W. Cassing, E. L. Bratkovskaya, V. P. Konchakovski and S. A. Voloshin, Phys. Rev. C **83**, 054911 (2011).
103. G. D. Moore and M. Tassler, JHEP **1102**, 105 (2011); G. D. Moore, hep-ph/0009161.
104. K. Fukushima and M. Ruggieri, Phys. Rev. D **82**, 054001 (2010).
105. R. Gatto and M. Ruggieri, Phys. Rev. D **85**, 054013 (2012).
106. M. Ruggieri, Phys. Rev. D **84**, 014011 (2011).
107. M. N. Chernodub and A. S. Nedelin, Phys. Rev. D **83**, 105008 (2011).
108. C. A. B. Bayona, K. Peeters and M. Zamaklar, JHEP **1106**, 092 (2011).
109. B. Abelev *et al.* [ALICE Collaboration], arXiv:1207.0900 [nucl-ex].